Automatic Ocular Artifact Correction in Electroencephalography for Neurofeedback

Cassandra Dumas[1][a], Marie Constance Corsi[1][b], Claire Dussard[1][c], Fanny Grosselin[1,2][d]
and Nathalie George[1,2][e]

[1]*Sorbonne Université, Institut du Cerveau, Paris Brain Institute, ICM, Inserm, CNRS, APHP,*
Hôpital de la Pitié Salpêtrière, Paris, France
[2]*Institut du Cerveau, ICM, Inserm, U1127, CNRS, UMR 7225, Sorbonne Université, CENIR,*
Centre MEG-EEG, Paris, France

Keywords: Electroencephalography, Artifact Removal Methods, Blind Source Separation, Brain-Computer Interfaces.

Abstract: Ocular artifacts can significantly impact electroencephalography (EEG) signals, potentially compromising the performance of neurofeedback (NF) and brain-computer interfaces (BCI) based on EEG. This study investigates if the Approximate Joint Diagonalization of Fourier Cospectra (AJDC) method can effectively correct blink-related artifacts and preserve relevant neurophysiological signatures in a pseudo-online context. AJDC is a frequency-domain Blind Source Separation (BSS) technique, which uses cospectral analysis to isolate and attenuate blink artifacts. Using EEG data from 21 participants recorded during a NF motor imagery (MI) task, we compared AJDC with Independent Component Analysis (ICA), a widely used method for EEG denoising. We assessed the quality of blink artifact correction, the preservation of MI-related EEG signatures, and the influence of AJDC correction on the NF performance indicator. We show that AJDC effectively attenuates blink artifacts without distorting MI-related beta band signatures and with preservation of NF performance. AJDC was calibrated once on initial EEG data. We therefore assessed AJDC correction quality over time, showing some decrease. This suggests that periodic recalibration may benefit long EEG recording. This study highlights AJDC as a promising real-time solution for artifact management in NF, with the potential to provide consistent EEG quality and to enhance NF reliability.

1 INTRODUCTION

Electroencephalography (EEG) enables the tracking of electrical activity in large neuronal populations at the scalp surface with millisecond-level precision. Due to its non-invasive nature and exceptional temporal resolution, EEG has become a cornerstone in medical diagnostics (Thomas et al., 2021), continuous health monitoring (Friedman et al., 2009), and brain-controlled device operation (Al-Quraishi et al., 2018). However, it faces significant challenges due to its sensitivity to various artifacts – originating from physiological, instrumental, and environmental sources – which can severely degrade signal quality (Tatum et al., 2011). This sensitivity necessitates

continuous artifact management, as real-time applications – such as Brain Computer Interface (BCI) and neurofeedback (NF) systems, which translate brain signals into commands – rely on reliable data for effective interaction and feedback (Lotte et al., 2015).

Eye blinks, particularly problematic during open-eye sessions, are among the most disruptive artifacts, because they produce high-amplitude fluctuations across scalp channels (Iwasaki et al., 2005). Although primarily concentrated in the delta (0.5 Hz – 4 Hz) and theta (4 Hz – 8 Hz) bands, these artifacts can also extend into the alpha (8 Hz – 13Hz) and beta (13 Hz – 30 Hz) bands (Hagemann & Naumann, 2001), thus compromising signal integrity across many

[a] https://orcid.org/0000-0002-5795-5700
[b] https://orcid.org/0000-0002-6262-5036
[c] https://orcid.org/0000-0002-7146-2486
[d] https://orcid.org/0000-0002-5512-8584
[e] https://orcid.org/0000-0002-1556-973X

frequencies of interest in human electrophysiology. Eye blinks have a distinctive spatial signature, affecting signals primarily in the frontal and prefrontal regions (Joyce et al., 2004). Thus, they can markedly interfere with and hinder the decoding of brain activity related to cognitive or motor tasks. Effective NF relies on the precise, real-time extraction of EEG indicators, often based on power within specific frequency bands. This extraction is essential for training individuals to modulate brain activity within these bands, supporting processes of self-regulation and learning (Omejc et al., 2019). While band-pass or notch filters are commonly used in signal processing, they cannot be applied in this context, as the blink-related artifactual activity overlaps with the frequency bands of interest. Accurate artifact filtering is therefore crucial, especially in NF protocols where EEG signals serve as the basis for feedback indicators. Inadequate handling of blink artifacts can disrupt feedback quality, negatively impacting NF training and real-time BCI performance by distorting signals during training and interfering with user control during live NF sessions (Jiang et al., 2019).

Several artifact correction methods are widely used in EEG signal processing, whether in real-time or offline mode. Among them, one can cite blind source separation (BSS) techniques, such as independent component analysis (ICA) (Makeig et al., 1996) frequency and time-frequency decomposition methods, such as wavelet decomposition (Zikov et al., 2002), regression-based approaches (Croft & Barry, 2000), and artifact subspace reconstruction (ASR) (Mullen et al., 2015).

Each method has strengths and limitations. On one hand, effective methods such as ICA, regression, and wavelet analysis require the manual intervention of experts for optimal denoising, limiting their suitability for real-time applications. ASR, on the other hand, is advantageous for real-time settings due to its ability to detect artifact components automatically. However, it demands a calibration phase of at least one minute with a clean signal, which can pose practical difficulties when expert oversight is unavailable, or calibration constraints are strict. Additionally, mere artifact rejection is not desirable in NF and BCI contexts, as these real-time applications cannot afford the loss of data, which would disrupt the continuity of feedback.

As Mumtaz et al., 2021 highlight, significant challenges remain in achieving effective real-time artifact correction. One key issue for BCI and NF applications is the development of online correction methods that are not only accurate but also quickly and easily applicable in diverse environments.

The purpose of this study is to evaluate the performance of a BSS technique, the Approximate Joint Diagonalization of Fourier Cospectra (AJDC) method (Congedo et al., 2008) for blink artifact correction and assess its suitability for use in real-time applications. AJDC is particularly promising because it offers the advantage of calibration on short data segments. We hypothesized that AJDC can effectively reduce ocular artifacts while preserving relevant neurophysiological signatures and that this performance can be maintained even under online constraints. To test these hypotheses, we compared AJDC with ICA, which is widely adopted and considered as a gold standard EEG denoising method. This comparison was performed on a database of motor-imagery (MI) based NF recordings from 21 subjects (Dussard et al., 2024). We analyzed, first, blink artifact reduction and, second, EEG signal preservation focusing on MI-related EEG signatures in the beta band. Third, we examined the consistency of NF performance with AJDC correction and the robustness of AJDC over time.

2 MATERIALS AND METHODS

2.1 Dataset and Preprocessing

2.1.1 Participants and EEG Acquisition

The data used in this study were the EEG data of 21 healthy participants (12 females, age: 28.5 ± 6.7 years [mean $\pm$ SD]), which had been recorded in a single-session NF study based on MI of the right hand (see Dussard et al., 2024 for details of the original study).

EEG was recorded with a 32-channel active electrode cap (ActiCAP Snap, Brain Products GmbH) and an actiCHamp Plus amplification system (Brain Products GmbH). The electrodes were positioned according to the extended international 10-20 system at the following sites: Fp1, Fp2, F7, F3, Fz, F4, F8, FT9, FC5, FC1, FC2, FC6, FT10, T7, C3, Cz, C4, T8, TP9, CP5, CP1, CP2, CP6, TP10, P7, P3, Pz, P4, P8, O1, O2, and Oz. The reference electrode was placed at Fz and the ground electrode at Fpz.

Electrode impedances were kept below 10 kΩ wherever possible (median across electrode and subjects = 11 ± 10 kΩ). During EEG recording, participants were seated 80 cm from a computer screen in a dimly lit Faraday room and were asked to avoid moving to minimize artifacts. EEG data were recorded with a sampling rate of 1 kHz and a DC-280 Hz bandpass filter, using the BrainVision recorder.

2.1.2 Experimental Protocol

The experiment included six NF runs under three different feedback modalities. Each run consisted of five trials of 30 seconds each, with a one-minute break between runs. During the trials, the participant performed MI of the right hand for 25 s (from t = 0 s to t = 25 s) while visual feedback reflecting the associated desynchronization in the EEG beta band (8-30 Hz) on the left central electrode C3 (located over the right-hand motor cortex) was displayed. This desynchronization, often observed in motor imagery tasks, reflects a decrease in beta power associated with the suppression of synchronized neural oscillations, particularly within the motor cortex (Pfurtscheller & Lopes da Silva, 1999). Intermittent vibratory tactile feedback was also delivered in two runs. The total duration of the NF session was approximately 20 minutes.

The NF task was preceded by a brief training phase consisting of three familiarization tasks, each lasting 30 seconds. These tasks included (1) observing a hand movement displayed on the screen, (2) performing an actual hand movement, and (3) imagining the hand movement while viewing it on the screen. This 1.5-min training phase was followed by 5 minutes of control tasks before starting the NF runs.

2.1.3 EEG Preprocessing

We re-referenced the EEG data with respect to an average reference across all electrodes, at each time point. We applied a 50 Hz-centered notch filter to attenuate mains frequency interference and a 0.5 Hz high-pass filter to remove slow drifts, using 4th-order, zero-phase, Butterworth filters as implemented in the MNE 1.8.0 package (Gramfort et al., 2014; Larson et al., 2024). Due to the presence of persistent muscle artifacts, two electrodes (FT9 and TP9) were excluded from the analyses.

2.2 Denoising Methods

We focused on BSS methods, since AJDC pertains to this family of methods.

2.2.1 Blind Source Separation Principle

BSS is a signal analysis technique commonly used in EEG signal processing to isolate neuronal sources of interest or to remove artifact sources, such as eye blinks or heartbeats, from cerebral activities (Delorme et al., 2007). It relies on the principle of statistical independence of the sources, which enables the identification and reconstruction of the signals of interest. The relationship between the multichannel EEG signal X and the underlying source signals, S, is modeled as follows:

$$X = A \cdot S \qquad (1)$$

Where A is the mixing matrix, representing the contributions of each source in each electrode.

The principle of BSS is to estimate the unmixing matrix B, using method-specific optimization criteria to reconstruct sources while minimizing dependencies between them:

$$S = B \cdot X \qquad (2)$$

with $B = A^{-1}$

2.2.2 AJDC-Based Denoising

AJDC operates on the principle of minimizing inter-source dependencies by diagonalizing cospectrum matrices across frequencies. This joint diagonalization isolates independent signal components by making the matrices as diagonal as possible, following several steps:

(a) *Frequency transformation*: The multi-channel EEG signal X is first transformed into the frequency domain. For each frequency f, the cospectrum matrix C_f is the matrix of covariance between EEG channels at this frequency:

$$C_f = Cov(X_f) \qquad (3)$$

(b) *Joint diagonalization*: AJDC uses a cost function $J(B)$ that measures the sum of the off-diagonal elements of the transformed cospectrum matrices, denoted D_f, as:

$$J(B) = \sum_f \sum_{i \neq j} |D_{f,ij}|^2 \qquad (4)$$

Where $D_{f,ij}$ represents the off-diagonal elements of each transformed matrix $D_f = BC_fB^T$, and B is the unmixing matrix. Minimizing $J(B)$ forces the matrices D_f to become quasi-diagonal, ensuring that the sources are independent of each other.

(c) *Application and source separation*: The estimated unmixing matrix B is then applied to separate sources. The source of blinks is then identified based on its spatial and temporal signatures, and it is set to 0 to reconstruct an artifact-free signal by applying A matrix (where $A = B^{-1}$) to the remaining source signals S.

One of the main advantages of AJDC is the rapid estimation of B. The method exploits the fact that EEG artifacts, such as eye blinks, exhibit stable spectral and spatial signatures over short time

periods. Thus, the rapid convergence of cospectrum matrices C_f provides a reliable estimate of B with a limited amount of data.

We implemented AJDC using the pyriemann 0.6 package (Barachant et al., 2024). To simulate real-time calibration and application, we used 20 seconds of the EEG signal recorded during hand observation in the training phase, to calibrate our B matrix, for each subject. We performed AJDC between 1 and 80 Hz, and the source of eye blink artifact (N=1 for each subject) was identified by an expert. The B matrix was then applied in non-overlapping sliding 500-ms time windows to the EEG data recorded during the calibration and the six NF runs.

2.2.3 ICA-Based Denoising

Unlike AJDC, which operates in the frequency domain, ICA separates sources by maximizing their statistical independence in the time domain. In this study, the FastICA algorithm was chosen due to its computational efficiency and robust performance for isolating artifacts in EEG data (Langlois et al., 2010). It is based on a fixed-point algorithm that iteratively maximizes non-Gaussianity, which serves as an indicator of statistical independence. The process comprises the following steps:

(a) *Preprocessing*: The EEG data matrix X requires an initial whitening step in ICA to decorrelate channels, simplifying the estimation of independent components. Whitening, or sphering, transforms the data to remove correlations between channels by performing an eigenvalue decomposition, where V is the matrix of eigenvectors and Λ is the diagonal matrix of eigenvalues. The whitened signal is then computed as:

$$X_{whitened} = \Lambda^{-\frac{1}{2}} V^T X \qquad (5)$$

This contrasts with AJDC that leverages cospectrum matrices in the frequency domain, which inherently contain reduced dependencies between channels. By jointly diagonalizing these matrices, AJDC further minimizes dependencies, bypassing the need for whitening and directly isolating sources based on their spectral characteristics.

(b) *Optimization*: Unlike AJDC, which uses a cost function to minimize the off-diagonal elements of transformed cospectrum matrices, FastICA maximizes source independence in the time domain by iteratively updating the unmixing matrix B based on non-Gaussianity. This measure of non-Gaussianity serves as an indicator of statistical independence, guiding FastICA to refine B until source independence is maximized.

(c) *Application and source separation*: As for AJDC, once the B matrix is estimated, artifactual components can be identified and removed, and the cleaned signal is reconstructed by applying A matrix to the remaining source signals S.

We implemented FastICA using the MNE 1.8.0 package (Gramfort et al., 2014; Larson et al., 2024). One major drawback of FastICA (and ICA in general) is the need for sufficiently long data segments to ensure reliable convergence and source estimation. Thus, we performed ICA decomposition on each of the six NF runs, as is standard in offline EEG data processing. The components corresponding to the eye blinks (N=1 or 2 for each subject) in each run were identified by an expert.

2.3 Evaluation of AJDC

2.3.1 Artifact Reduction

To assess the effectiveness of blink artifact correction, we compared the blink Evoked Potentials (EPs) recorded on each electrode in the raw data and after correction with AJDC or ICA. Blink events were automatically detected on the raw data using the *find_eog_events* function (with default parameters and Fp1 and Fp2 as EOG references) from the MNE package, centering the analysis on epochs of ±500ms around the blink peaks. The same events were then aligned with the data processed by AJDC and ICA. Blink EPs were obtained by averaging all blink epochs in each subject. Power Spectral Densities (PSDs) were estimated between 1 and 80 Hz using the multitaper method with Discrete Prolate Spheroidal Sequence (DPSS) across all blink epochs and then averaged. For illustration purposes, the PSDs were averaged over three regions – frontal (Fp1, Fp2, F7, F3, Fz, F4, F8), central (FC5, FC1, FC2, FC6, FT10, T7, C3, Cz, C4, T8, CP5, CP1, CP2, CP6, TP10), and posterior (P7, P3, Pz, P4, P8, O1, Oz, O2) – and the EP and PSD data were averaged across subjects.

2.3.2 Preservation of MI Signatures

At the electrophysiological level, we assessed event-related desynchronization / synchronization (ERD/ERS) across frequencies throughout the NF runs, for the RAW, AJDC-, and ICA-corrected data. For each participant, EEG signals were segmented into NF trials (from t = -5 s to t = 30 s, where 0 was the start of the NF period). Trials with muscle artifacts were visually inspected and excluded. We used Morlet wavelets (with a 500 ms width) to transform the data in the time-frequency domain
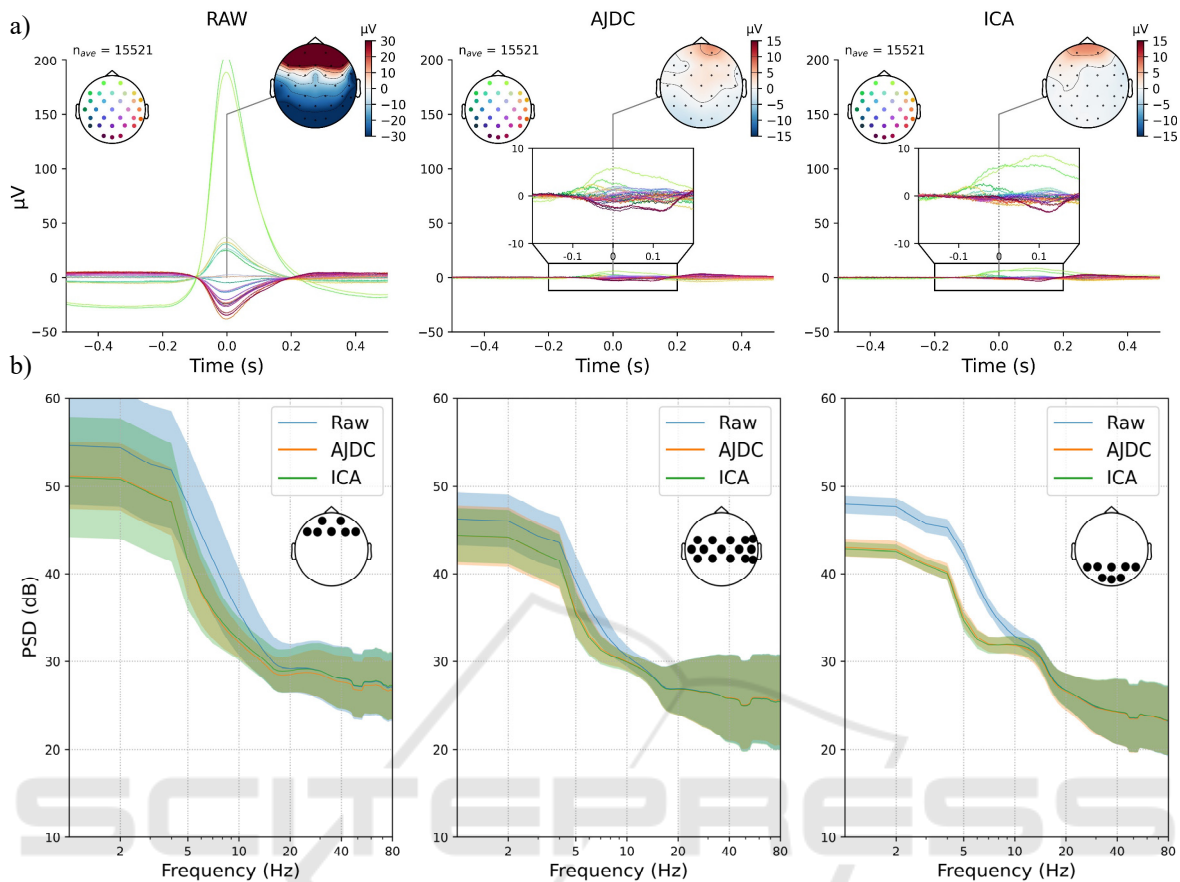
Figure 1: Artefact Reduction. (a) Blink EPs for the conditions: RAW (left), AJDC-corrected (centre), ICA-corrected (right) signals. The grand average of the EPs across subjects is presented. At the top of each plot, topographies represent the spatial distribution of the blink EPs at t = 0 s corresponding to the blink peak. The inset boxes zoom in on the corrected EPs for better visualization of the differences between methods. Vertical axis: amplitude (µV); horizontal axis: time (s). (b) Power spectra averaged on three scalp regions (from left to right: frontal, central, posterior) and averaged across subjects. Spectra derived from raw signals are represented in blue, those from AJDC-corrected blink epochs in orange, and those from ICA-corrected blink epochs in green. The lighter shaded area around each PSD represents the standard deviation across subjectts. Vertical axis: spectral amplitudes (dB) ; horizontal axis: frequencies (Hz). An inset on each plot shows the electrodes that were included in each scalp region.

between 1 Hz and 80 Hz, with 0.5 Hz frequency bins. The wavelet cycles were linearly scaled with frequency to ensure consistent time-frequency resolution. Morlet wavelets were chosen for their optimal trade-off between temporal and spectral resolution (Bertrand et al., 2000). This approach ensures precise characterization of both low- and high-frequency bands while preserving consistent temporal accuracy across the entire frequency range. The trials were averaged, and the signal power was then baseline-corrected using a log-ratio, with each time point corrected relative to the mean power during a 2-s fixation period (from t = -3 s to t = -1 s).

Furthermore, to check the preservation of MI signatures after AJDC relative to ICA correction, we employed Representational Similarity Analysis (RSA) (Kriegeskorte et al., 2008) of the topographical patterns. For each participant, we constructed dissimilarity matrices from the MI-related topographical maps after AJDC and after ICA, respectively, by computing pairwise Euclidean distances between electrode pairs. The similarity between these matrices was then assessed using Spearman's rank correlation coefficient. By leveraging RSA – which combines the computation of dissimilarity matrices and their subsequent correlation – we quantitatively assessed whether the topographical structure of MI patterns was maintained across different correction methods.
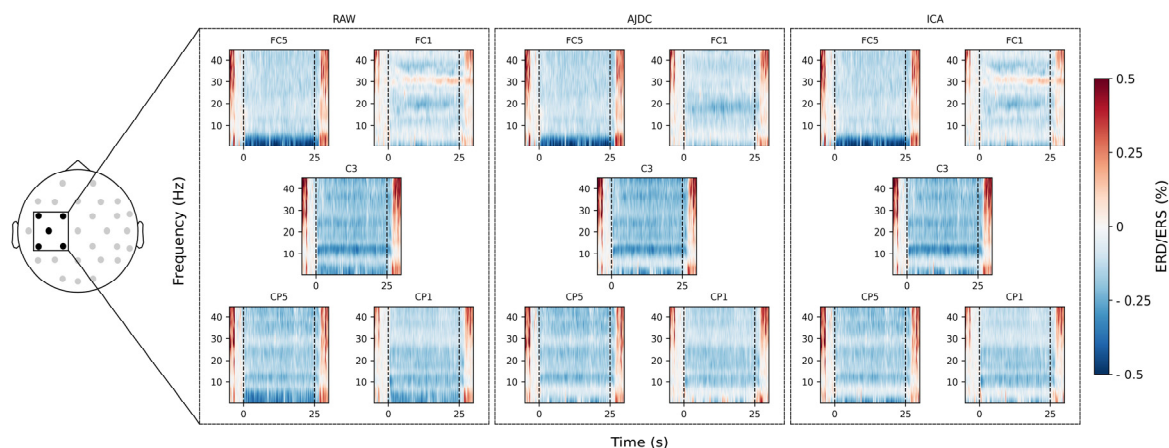
Figure 2: Preservation of MI signatures. Time-frequency representation of EEG power on each electrode of the Laplacian filter in RAW, AJDC and ICA conditions, during the NF trials. The grand average of the data across subjects is represented. The thin black dashed lines at 0 and 25 s represent the start and end of NF during the trials. ERD/ERS values are color coded, with the blue colors representing ERD and the red colors representing ERS. Vertical axis: frequencies (Hz) ; horizontal axis: time (s).

2.3.3 Simulation of Online Application

To quantify the beta-band (β) activity that participants aimed to regulate through NF in a pseudo-online fashion (aka. NF performance), we used the OpenViBE 2.2.0 (Renard et al., 2010) processing pipeline applied during the experiment. This pipeline calculated online β power (*online β*), during NF trials and compared it to a reference β power (*reference β*). A Laplacian spatial filter was applied to electrode C3 by subtracting signals from adjacent electrodes (CP5, CP1, FC1, and FC5). The resulting signal was band-pass filtered between 8 and 30 Hz using an 8th-order Butterworth filter, then segmented into 1 s epochs with a 0.75 s overlap. For each epoch, β power was calculated by squaring and averaging the signal. *Online β* was derived by averaging β power values over the 4 epochs preceding each feedback cycle during the NF runs (see Dussard et al., 2024 for details). It was compared to a common *reference β* power value derived from a 60 s baseline period recorded before the NF task. This *reference β* was calculated by averaging the median β power of the AJDC-corrected baseline period and the median β power of the RAW baseline period.

NF performance was then computed as follows. Each trial included 16 feedback cycles based on 16 *online β* values, which were compared to the participant's *reference β*. We divided each *online β* value by the *reference β* and computed the median of these 80 ratios (16 values per trial × 5 trials per run) for every NF run. The result was log-transformed, with the sign inverted, so that positive values

indicated a reduction in *online β* relative to *reference β*, thus reflecting successful NF performance.

Finally, since AJDC was calibrated at the beginning of the experiment and applied throughout the NF runs, we also examined the quality of the correction over time. To do this, we extracted a signal-to-noise ratio (SNR) of the blink EPs, calculated across the NF runs as follows:

$$SNR = -10 \log \left(\frac{signal_{AJDC}}{signal_{RAW}} \right) \quad (6)$$

2.3.4 Statistical Analyses

(1) For *artifact reduction* analysis, PSD values of blink epochs on each electrode and at each frequency (1 to 80 Hz) were compared between ICA and AJDC corrections.

(2) For *MI-related signature preservation* analysis, power in the frequency band and electrodes of interest (that is, 8-30 Hz band on FC1, FC5, C3, CP1, and CP5) was averaged and compared 2-by-2 between the RAW, AJDC, and ICA conditions.

(3) For *SNR* analysis, SNR values on each electrode were compared between the first and last NF runs, which were separated by an interval of 15-20 minutes.

When relevant, normality was assessed with the Shapiro-Wilk test. When normality was met, paired t-tests across subjects were used; otherwise, we used Wilcoxon signed-rank tests. For each analysis, the p-values were corrected for multiple comparisons using the False Discovery Rate (FDR) correction from Benjamini-Hochberg (Benjamini & Hochberg, 1995), with FDR-corrected significance level (pFDR) set at 0.05.

3 RESULTS

3.1 Artifact Reduction

We first investigated the artifact reduction resulting from AJDC and ICA. For this purpose, we compared the blink EPs averaged from RAW signals and from signals corrected by AJDC and ICA. (see Figure 1.a). Both correction methods visibly reduced blink artifacts, as shown in the topographies at t = 0 s corresponding to the peak of the blink artifact, though some frontal activity remained present in the corrected signals. Focusing on frontal electrodes (Fp1, Fp2, F7, F3, Fz, F4, F8), the average artifact amplitude reduction was of 75.88 µV (± 24.28 µV; [mean ± SD]) for AJDC and 75.56 µV (± 23.49 µV; [mean ± SD]) for ICA. The differences between AJDC and ICA seemed minimal, with only slight variations in the spatial distribution and intensity of residual activity.

To further investigate the effects of AJDC and ICA on artifact reduction, we analyzed the PSD averaged from blink epochs across frontal, central, and posterior regions for both raw and corrected signals (see Figure 1.b). A slight divergence between AJDC- and ICA-corrected PSDs emerged only in the frontal region, particularly at frequencies above 10 Hz. However, AJDC- and ICA- corrected PSDs did not show any significant difference on either electrode or frequency (all pFDR > 0.05).

3.2 Preservation of MI Signatures

We investigated the extent to which the AJDC preserved neurophysiological information of interest despite the ocular artifact removal. Figure 2 shows the time-frequency representation of the targeted beta ERD during the NF trials, across the electrodes involved in the Laplacian filter (that was used during the NF protocol, see Methods). Both correction methods appeared to preserve a similar MI-related signature, except for electrode FC1 were a high-frequency activity (around 30 Hz) was present in RAW and ICA-corrected data but absent in AJDC-corrected data. Some weak differences between AJDC- and ICA-corrected time-frequency representations were also visible in the low-frequency range (<5 Hz) on CP1. Yet, the comparison of the mean ERD in the beta band (8-30 Hz) between 0 and 25 s on the five-electrode involved in the Laplacian computation did not show any statistically significant 2-by-2 difference between RAW, AJDC-corrected and ICA-corrected data (pFDR > 0.05).

Furthermore, RSA analysis revealed a mean similarity score of 0.87 ± 0.07 ([mean ± SD]), indicating a preservation of the topographical structure of MI patterns across the AJDC and ICA correction methods.
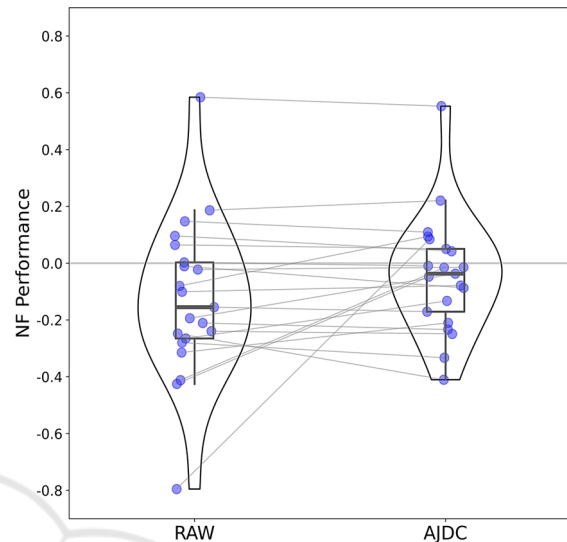

Figure 3: Comparison of NF performance between RAW and AJDC conditions. Blue dots represent individual data. For each condition, the thick horizontal black line is the median value across subjects, the box plot corresponds to the second and third quartiles, and the vertical these black lines correspond to the lower and upper quartiles (excluding outlier values). Violin plots of the individual data are also included. Vertical axis: NF performance; horizontal axis: conditions.

3.3 Simulation of Online Application

We evaluated the potential impact of AJDC on NF performance in a pseudo-online framework, replaying the data in real-time in OpenVibe to simulate live recording conditions. Analysis of RAW versus AJDC-corrected neurofeedback performance showed no significant effect, with pFDR > 0.05.

0Moreover, to evaluate the consistency of the AJDC correction over time, we compared SNR values between the first and last NF runs (see Figure 4). A general decrease in SNR was observed across electrodes, with lower SNR values in the last run compared to the first one. Statistical analysis revealed significant SNR differences on three electrodes (F3, F8 and FC5; pFDR < 0.05). However, this did not seem to impact NF performance insofar as there was no significant difference between the delta of NF performance between AJDC and RAW in the first run and the delta of NF performance between AJDC and RAW in the last run (pFDR > 0.05).
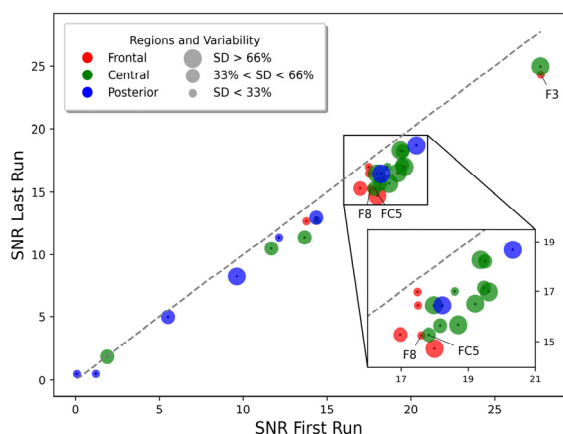
Figure 4: Difference in SNR between the first and last NF runs for each electrode. The electrodes are colored according to their scalp region: frontal (red), central (green), and posterior (blue), corresponding to the same regions as in Figure 2. The size of the colored circle reflects the variability (standard deviation, SD) of the first vs. last run SNR difference across subjects. For visualization purpose, 3 circle size are represented: the larger circles represent the electrodes with a SD of SNR difference belonging to the 66% higher percentile of all SD values across electrodes, the medium size circles represent the electrodes with a SD value between 33% and 66% of all SD values, and smaller circles represent electrodes with a SD less than 33% of all SD values.

4 DISCUSSION

In NF and BCI, ocular artifacts – particularly those from eye blinks – present a substantial challenge, as they can severely distort EEG signatures. This study evaluated the efficacy of the AJDC method for automatic blink artifact correction in EEG data, benchmarking it against the well-known ICA.

Our study showed that AJDC effectively reduces blink artifacts in EEG signals, notably by attenuating the frontal blink-related activity, which often disrupts BCI and NF applications (Jiang et al., 2019). This result aligns with expectations, as blink artifacts are known to predominantly impact frontal channels due to their proximity to the ocular sources (Joyce et al., 2004). Although both AJDC and ICA methods offered comparable performance, minor differences appeared in high frequencies (>10 Hz) in the frontal regions, where AJDC exhibited a correction profile distinct from ICA. In the PSD analysis, the mean PSD across scalp regions and subjects was lower for AJDC compared to ICA; ICA PSD was closer to the RAW PSD. This slight variation may reflect specific characteristics of the AJDC decomposition process,

potentially influencing the spectral content (Congedo et al., 2008). Although these differences did not reach statistical significance, they may reflect unique characteristics of AJDC correction. These observations align with the conclusions of Barthélemy et al., 2017, who demonstrated that AJDC can effectively isolate and reduce ocular artifacts. They also found minor differences between manual denoising by ICA and automatic denoising by AJDC in the PSD of frontal electrodes, suggesting that AJDC may offer a distinct profile in terms of power distribution in this region.

Beyond artifact reduction, we also considered the AJDC method's ability to preserve essential neurophysiological information of interest, that is, here, ERD in the beta band. In this regard, AJDC seemed to preserve MI-related activity within the 8-30 Hz band; there was no evidence of signal deformation in this frequency range (see Figure 2). This observation is in line with the findings from Barthélemy et al., 2017, who demonstrated that event-related potentials (ERPs) remained unaffected by distortions from AJDC correction, supporting its suitability for preserving key neural signals. That said, some difference was observed around 30Hz on electrode FC1. We went back to individual data and noted that this difference was attributable to a single subject who exhibited a high fluctuation in EEG activity at this frequency. This fluctuation was absent in the AJDC calibration data and therefore picked up to some extent in the ocular component targeted for removal during the NF runs. This outcome suggests that while AJDC is robust in most cases, subject-specific EEG variations or outliers may lead to unanticipated inclusions in the correction process. This is further supported by the RSA scores, which indicated an average similarity above 85%. While this represents a high degree of similarity, it is not perfect (i.e., not 100%), suggesting the presence of residual differences. Such variations can influence the motor signature by introducing unintended corrections. This observation resonates with findings from prior studies, which emphasized the challenges posed by intra-subject variability in EEG and artifact correction methods (Ronca et al., 2024; Wei et al., 2021).

In terms of NF performance, no significant difference was found between the RAW and AJDC-corrected conditions in a pseudo-online framework, where data were replayed in real-time in OpenVibe to simulate live recording conditions (see Figure 3). For the purpose of this analysis, a common *reference β* power was used for both methods, calculated as the mean of the *reference β* power from each method.

However, we checked that a method-specific *reference β* did not alter our conclusions. This is consistent with the findings of Dussard et al., 2024, who demonstrated that Laplacian techniques are resilient to ocular artifacts. It is however worth noting that more complex spatial filtering methods that integrate information from the entire scalp, such as Common Spatial Patterns (CSP) (Blankertz et al., 2008), are more sensitive to ocular artifacts, potentially impacting their performance. CSPs are commonly used in BCI protocols due to their effectiveness in discriminating MI-related EEG patterns, yet they are sensitive to ocular artifacts that can degrade their accuracy if not adequately managed (Jafarifarmand & Badamchizadeh, 2019). AJDC may be particularly useful in the context of CSP and other advanced feature extraction methods.

In addition to the overall performance analysis, a notable aspect of our results is the observed progressive decline in the effectiveness of AJDC correction over the course of the experiment (see Figure 4). This trend suggests that periodic adjustments or recalibrations may be necessary to sustain the AJDC method efficacy. This temporal degradation likely arises from dynamic changes in artifact characteristics and neural signal properties (Ambrogioni et al., 2017; Islam et al., 2021). This observation is in agreement with broader findings in the literature on BCI and NF systems, where maintaining stable performance across time is often challenging due to various sources of signal variability, including changes in electrode impedance, user fatigue, and cognitive state fluctuations (Alkoby et al., 2018; Saha & Baumert, 2020; Vidaurre & Blankertz, 2010). Such fluctuations can impact the consistency of the neural signals, thereby complicating real-time processing and artifact correction. An improvement to the AJDC method could involve implementing a real-time, offset calibration, where a new correction matrix is recalculated in the background during real-time artifact correction.

While the AJDC method shows promising results in blink artifact correction, certain limitations remain. First, AJDC requires manual identification of artifacts components, a step conducted at the beginning of the experiment in our protocol. While this initial calibration minimizes variability, it relies on expert input, which introduces inter-operator variability and limits reproducibility across different experimental setups (Barthélemy et al., 2017). Additionally, although our study focused solely on blink artifacts, a multitude of other artifact types – including physiological (e.g. muscle activity) and environmental noise – can significantly impact EEG signals (Tatum et al., 2011). The efficacy of AJDC for these types of artifacts has yet to be assessed comprehensively, as various studies highlight the importance of robust correction methods for diverse EEG artifacts to ensure signal integrity in BCI applications (McDermott et al., 2022).

Another limitation is the offline nature of our comparison. While this approach was justified by the shared BSS framework of both AJDC and ICA methods, it would be interesting to also test AJDC against a real-time method, such as ASR (Mullen et al., 2015), for a fuller methodological benchmark. This comparison is particularly relevant for BCI and NF applications, where continuous adaptation and real-time processing are critical (Saha & Baumert, 2020). Our comparison with ICA is valuable given the well-documented strengths and limitations of ICA in artifact correction. Another interesting suggestion could be to test AJDC on clean EEG data artificially contaminated with controlled artifacts (Chavez et al., 2018). This approach would allow for a rigorous evaluation of AJDC artifact correction efficacy and its impact on neural signals. Furthermore, such a setup would enable the exploration of additional metrics, such as phase delay, relative root mean square error, coherence or Riemannian distance. These measures could provide complementary insights into the quality of artifact correction.

Finally, this study serves as a proof of concept, demonstrating the potential of the AJDC method in comparison to ICA using data from healthy subjects. However, to fully assess the robustness and clinical applicability of AJDC, it would be essential to evaluate its performance on patients' data. Patients' populations may exhibit more pronounced artifacts due to various factors such as increased physiological variability, medication effects, or underlying neurological conditions (Karson, 1983; Kimura et al., 2017). Evaluating AJDC on such data would provide critical insights into its efficacy in real-world clinical contexts.

In summary, our study offers a promising first step toward robust real-time EEG artifact correction with AJDC, highlighting areas for further development in automating and validating the method across diverse recording conditions and artifact types.

REFERENCES

Alkoby, O., Abu-Rmileh, A., Shriki, O., & Todder, D. (2018). Can We Predict Who Will Respond to Neurofeedback? A Review of the Inefficacy Problem

and Existing Predictors for Successful EEG Neurofeedback Learning. *Neuroscience*, *378*, 155–164.

Al-Quraishi, M. S., Elamvazuthi, I., Daud, S. A., Parasuraman, S., & Borboni, A. (2018). EEG-Based Control for Upper and Lower Limb Exoskeletons and Prostheses: A Systematic Review. *Sensors (Basel, Switzerland)*, *18*, 3342.

Ambrogioni, L., Gerven, M. A. J. van, & Maris, E. (2017). Dynamic decomposition of spatiotemporal neural signals. *PLOS Computational Biology*, *13*(5).

Barachant, A., Barthélemy, Q., Wagner vom Berg, G., Gramfort, A., King, J.-R., & Rodrigues, P. L. C. (2024). *pyRiemann/pyRiemann: V0.6* (Version v0.6) [Computer software].

Barthélemy, Q., Mayaud, L., Renard, Y., Kim, D., Kang, S.-W., Gunkelman, J., & Congedo, M. (2017). Online denoising of eye-blinks in electroencephalography. *Clinical Neurophysiology*, *47*(5–6), 371–391.

Benjamini, Y., & Hochberg, Y. (1995). Controlling the False Discovery Rate: A Practical and Powerful Approach to Multiple Testing. *Journal of the Royal Statistical Society: Series B (Methodological)*, *57*(1), 289–300.

Bertrand, O., Tallon-Baudry, C., & Pernier, J. (2000). *Time-Frequency Analysis of Oscillatory Gamma-Band Activity: Wavelet Approach and Phase-Locking Estimation* (Vol. 2, pp. 919–922).

Blankertz, B., Tomioka, R., Lemm, S., Kawanabe, M., & Muller, K. (2008). Optimizing Spatial filters for Robust EEG Single-Trial Analysis. *IEEE Signal Processing Magazine*, *25*(1), 41–56.

Chavez, M., Grosselin, F., Bussalb, A., De Vico Fallani, F., & Navarro-Sune, X. (2018). Surrogate-Based Artifact Removal From Single-Channel EEG. *IEEE Transactions on Neural Systems and Rehabilitation Engineering*, *26*(3), 540–550.

Congedo, M., Gouy-Pailler, C., & Jutten, C. (2008). On the blind source separation of human electroencephalogram by approximate joint diagonalization of second order statistics. *Clinical Neurophysiology*, *119*(12), 2677–2686.

Croft, R. J., & Barry, R. J. (2000). EOG correction of blinks with saccade coefficients: A test and revision of the aligned-artefact average solution. *Clinical Neurophysiology*, *111*(3), 444–451.

Delorme, A., Sejnowski, T., & Makeig, S. (2007). Enhanced detection of artifacts in EEG data using higher-order statistics and independent component analysis. *NeuroImage*, *34*(4), 1443–1449.

Dussard, C., Pillette, L., Dumas, C., Pierrieau, E., Hugueville, L., Lau, B., Jeunet-Kelway, C., & George, N. (2024). Influence of feedback transparency on motor imagery neurofeedback performance: The contribution of agency. *Journal of Neural Engineering*, *21*(5).

Friedman, D., Claassen, J., & Hirsch, L. J. (2009). Continuous electroencephalogram monitoring in the intensive care unit. *Anesthesia and Analgesia*, *109*(2), 506–523.

Gramfort, A., Luessi, M., Larson, E., Engemann, D. A., Strohmeier, D., Brodbeck, C., Parkkonen, L., &

Hämäläinen, M. S. (2014). MNE software for processing MEG and EEG data. *NeuroImage*, *86*, 446–460.

Hagemann, D., & Naumann, E. (2001). The effects of ocular artifacts on (lateralized) broadband power in the EEG. *Clinical Neurophysiology*, *112*(2), 215–231.

Islam, Md. K., Rastegarnia, A., & Sanei, S. (2021). Signal Artifacts and Techniques for Artifacts and Noise Removal. In *Signal Processing Techniques for Computational Health Informatics* (Vol. 192, pp. 23–79). Springer.

Iwasaki, M., Kellinghaus, C., Alexopoulos, A. V., Burgess, R. C., Kumar, A. N., Han, Y. H., Lüders, H. O., & Leigh, R. J. (2005). Effects of eyelid closure, blinks, and eye movements on the electroencephalogram. *Clinical Neurophysiology*, *116*(4), 878–885.

Jafarifarmand, A., & Badamchizadeh, M. A. (2019). EEG Artifacts Handling in a Real Practical Brain–Computer Interface Controlled Vehicle. *IEEE Transactions on Neural Systems and Rehabilitation Engineering*, *27*(6), 1200–1208.

Jiang, X., Bian, G.-B., & Tian, Z. (2019). Removal of Artifacts from EEG Signals: A Review. *Sensors (Basel, Switzerland)*, *19*(5), 987.

Joyce, C. A., Gorodnitsky, I. F., & Kutas, M. (2004). Automatic removal of eye movement and blink artifacts from EEG data using blind component separation. *Psychophysiology*, *41*(2), 313–325.

Karson, C. N. (1983). Spontaneous Eye-Blinks Rates and Dopaminergic Systems. *Brain*, *106*(3), 643–653.

Kimura, N., Watanabe, A., Suzuki, K., Toyoda, H., Hakamata, N., Fukuoka, H., Washimi, Y., Arahata, Y., Takeda, A., Kondo, M., Mizuno, T., & Kinoshita, S. (2017). Measurement of spontaneous blinks in patients with Parkinson's disease using a new high-speed blink analysis system. *Journal of the Neurological Sciences*, *380*, 200–204.

Kriegeskorte, N., Mur, M., & Bandettini, P. A. (2008). Representational similarity analysis—Connecting the branches of systems neuroscience. *Frontiers in Systems Neuroscience*, *2*.

Langlois, D., Chartier, S., & Gosselin, D. (2010). An Introduction to Independent Component Analysis: InfoMax and FastICA algorithms. *Tutorials in Quantitative Methods for Psychology*, *6*(1), 31–38.

Larson, E., Gramfort, A., Engemann, D. A., Leppakangas, J., Brodbeck, C., Jas, M., Brooks, T. L., Sassenhagen, J., McCloy, D., Luessi, M., King, J.-R., Höchenberger, R., Goj, R., Favelier, G., Brunner, C., van Vliet, M., Wronkiewicz, M., Rockhill, A., Holdgraf, C., … luzpaz. (2024). *MNE-Python* (Version v1.8.0) [Computer software].

Lotte, F., Bougrain, L., & Clerc, M. (2015). Electroencephalography (EEG)-Based Brain–Computer Interfaces. In J. G. Webster (Ed.), *Wiley Encyclopedia of Electrical and Electronics Engineering* (1st ed., p. 44). Wiley.

Makeig, S., Bell, A., Jung, T.-P., & Sejnowski, T. (1996). Independent Component Analysis of Electroencephalo-

graphic Data. *Advances in Neural Information Processing Systems*, *8*.

McDermott, E. J., Raggam, P., Kirsch, S., Belardinelli, P., Ziemann, U., & Zrenner, C. (2022). Artifacts in EEG-Based BCI Therapies: Friend or Foe? *Sensors*, *22*(1), 96.

Mullen, T. R., Kothe, C. A. E., Chi, Y. M., Ojeda, A., Kerth, T., Makeig, S., Jung, T.-P., & Cauwenberghs, G. (2015). Real-Time Neuroimaging and Cognitive Monitoring Using Wearable Dry EEG. *IEEE Transactions on Bio-Medical Engineering*, *62*(11), 2553–2567.

Mumtaz, W., Rasheed, S., & Irfan, A. (2021). Review of challenges associated with the EEG artifact removal methods. *Biomedical Signal Processing and Control*, *68*, 102741.

Omejc, N., Rojc, B., Battaglini, P. P., & Marusic, U. (2019). Review of the therapeutic neurofeedback method using electroencephalography: EEG Neurofeedback. *Bosnian Journal of Basic Medical Sciences*, *19*(3), 213–220.

Pfurtscheller, G., & Lopes da Silva, F. H. (1999). Event-related EEG/MEG synchronization and desynchronization: Basic principles. *Clinical Neurophysiology*, *110*(11), 1842–1857.

Renard, Y., Lotte, F., Gibert, G., Congedo, M., Maby, E., Delannoy, V., Bertrand, O., & Lécuyer, A. (2010). OpenViBE: An Open-Source Software Platform to Design, Test, and Use Brain–Computer Interfaces in Real and Virtual Environments. *Presence*, *19*(1), 35–53.

Ronca, V., Capotorto, R., Di Flumeri, G., Giorgi, A., Vozzi, A., Germano, D., Virgilio, V. D., Borghini, G., Cartocci, G., Rossi, D., Inguscio, B. M. S., Babiloni, F., & Aricò, P. (2024). Optimizing EEG Signal Integrity: A Comprehensive Guide to Ocular Artifact Correction. *Bioengineering*, *11*(10), 1018.

Saha, S., & Baumert, M. (2020). Intra- and Inter-subject Variability in EEG-Based Sensorimotor Brain Computer Interface: A Review. *Frontiers in Computational Neuroscience*, *13*, 87.

Tatum, W. O., Dworetzky, B. A., & Schomer, D. L. (2011). Artifact and Recording Concepts in EEG. *Journal of Clinical Neurophysiology*, *28*(3), 252–263.

Thomas, J., Thangavel, P., Peh, W. Y., Jing, J., Yuvaraj, R., Cash, S. S., Chaudhari, R., Karia, S., Rathakrishnan, R., Saini, V., Shah, N., Srivastava, R., Tan, Y.-L., Westover, B., & Dauwels, J. (2021). Automated Adult Epilepsy Diagnostic Tool Based on Interictal Scalp Electroencephalogram Characteristics: A Six-Center Study. *International Journal of Neural Systems*, *31*(5), 2050074.

Vidaurre, C., & Blankertz, B. (2010). Towards a Cure for BCI Illiteracy. *Brain Topography*, *23*(2), 194–198.

Wei, C.-S., Keller, C. J., Li, J., Lin, Y.-P., Nakanishi, M., Wagner, J., Wu, W., Zhang, Y., & Jung, T.-P. (2021). Editorial: Inter- and Intra-subject Variability in Brain Imaging and Decoding. *Frontiers in Computational Neuroscience*, *15*, 791129.

Zikov, T., Bibian, S., Dumont, G. A., Huzmezan, M., & Ries, C. R. (2002). A wavelet based de-noising technique for ocular artifact correction of the electroencephalogram. *24th Annual Conference of the Biomedical Engineering Society*, *1*, 98–105 vol.1.